

Design and Calibration of a Small Aeroacoustic Beamformer

Elias J. G. Arcondoulis, Con J. Doolan, Anthony C. Zander and Laura A. Brooks

School of Mechanical Engineering, The University of Adelaide, Adelaide, Australia

PACS: 43.28.Ra, 43.58.Vb, 43.60.Fg.

ABSTRACT

The use of aeroacoustic beamforming has increased dramatically in the past decade. The primary driving force behind this has been the need to improve the noise characteristics of aircraft and automotive vehicles, coupled with ever increasing computer processing power. Aeroacoustic beamforming is an experimental technique that uses an array of microphones located in the far field of acoustic noise sources generated by a body in air flow. Each microphone measures an acoustic magnitude and relative phase based on its unique position with respect to the acoustic source(s). Beamforming algorithms process this data, typically to generate spatial noise source plots over a two dimensional grid at each frequency of interest. Much of the available aeroacoustic beamforming literature presents results at relatively high frequencies corresponding to large facilities, scale models, and available budgets, which can potentially set unrealistic goals for the development of a small-scale university research facility. This paper details the design and calibration of a small aeroacoustic beamformer, designed to investigate airfoil trailing edge noise for low to moderate Reynolds number flows. The optimisation of the microphone array, based on spatial, air flow and financial constraints, is presented. The algorithms which were used to calculate the beamformer outputs are described, as well as the array calibration process, including beamforming of various noise sources in an anechoic environment. The array is shown to successfully detect and accurately locate both tonal and broadband noise sources.

INTRODUCTION

Aeroacoustic beamforming is a relatively new application of phased array technology. It has been used successfully for the study of airfoil trailing edge noise (Brooks and Humphreys, 2006a, Dobrzyński et al., 2008 and Oerlemans et al., 2009) and aircraft landing gear (Dobrzyński et al., 2008).

The University of Adelaide is developing an advanced aeroacoustic test facility and is currently installing an aeroacoustic beamformer, primarily to study airfoil trailing edge noise at low to moderate Reynolds number (Arcondoulis et al., 2009). It is to be placed in The University of Adelaide's Anechoic Wind Tunnel (AWT). Figure 1 depicts the future aeroacoustic testing configuration in the AWT, using both beamforming and hot-wire anemometry (Arcondoulis et al., 2009). The distance of the acoustic beamformer to the airfoil trailing edge is approximately 600mm.

The dimensions of the AWT prohibit the installation of a large beamforming array. Underbrink (2002) recommends the use of logarithmic spiral arrays to optimise the use of a given number of microphones. However, to achieve high quality beamforming results using a small array, a new type of microphone arrangement was designed. It is a subtle modification to a logarithmic spiral, called the "Arcondoulis" spiral in this paper, after the first author who invented it. This spiral array exhibits improved sidelobe characteristics for the same number of microphones for a given square array area.

This paper provides a description of aeroacoustic beamforming and the algorithms required to process microphone array data. The design and optimisation of the beamforming array is presented along with a comparative analysis of the loga-

rithmic and Arcondoulis spirals. Experimental and simulated beamforming results using tonal and broadband noise sources for a 16 channel microphone array are presented, using both the Cross-Spectral and DAMAS (Deconvolution Approach for the Mapping of Acoustic Sources) (Brooks and Humphreys, 2006a) beamforming algorithms.

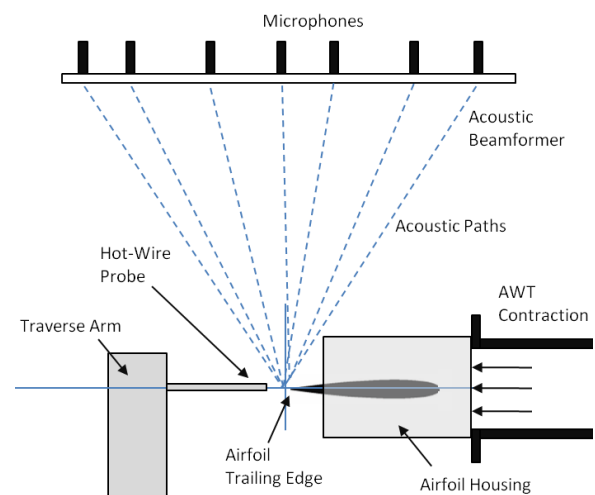


Figure 1: Schematic diagram of aeroacoustic beamforming of an airfoil in the AWT, University of Adelaide, Adelaide.

BEAMFORMING THEORY

Beamforming is a signal processing technique used in sensor arrays for directional signal transmission or reception. Its applications include radio astronomy, seismology and aeroacoustics, the field of interest here.

When a plane wave radiates towards a non-coplanar surface, each location on the plane will receive the wave with different acoustic phase. This is due to differences in propagation distance of the wave to each point. If microphones are placed on this non-coplanar surface, they will detect this unique acoustic magnitude and phase. A beamforming algorithm will scan a defined area of space to determine any noise sources. The direction of each area scan is called the focus direction. When the focus direction coincides with the incoming noise, a noise source is then detected (Brüel & Kjær, 2004). Figure 2 is a sensitivity diagram that shows a plane wave noise source distribution.

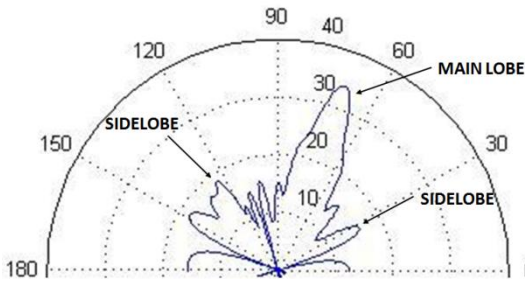


Figure 2: Sensitivity diagram (shown in dB, for various focus angles, in degrees) for a 63 channel array (Arcondoulis spiral, shown in Figure 3). The test source was a 7000Hz plane wave, arriving from the 70° direction.

The incident wave is non-coplanar with the microphone array plane, resulting in a sensitivity diagram that shows a noise source at an angle from the perpendicular axis of the array. Note that the “main lobe”, corresponding to the incoming wave source magnitude and direction, is not the only signal presented in Figure 2. There exist other signal patterns in other directions of noticeable magnitude called “sidelobes”. These are false spatial aliasing images which can potentially corrupt the quality of the source pressure distribution (Underbrink, 2002, Brüel & Kjær, 2004, Dougherty, 2005 and Brooks and Humphreys, 2006a,b).

Beamforming Algorithms

The sensitivity diagram acts as a test for the microphone array pattern, showing the effectiveness of the array to isolate a single incident wave (Brüel & Kjær, 2004). While an effective array design can reduce sidelobe images from sensitivity diagrams, the full ability of the array is not quantified from this measure alone. The need to further reduce sidelobe images in aeroacoustics has led to advances in beamforming techniques and algorithms, including Delay and Sum, Cross-Spectral and DAMAS. The following mathematical representation is adapted from Brüel & Kjær (2004) and Brooks and Humphreys (2006a).

Both the Delay and Sum and Cross-Spectral beamforming algorithms require a complex pressure magnitude and phase at each microphone. This data is processed first in the beamforming algorithm, in a Cross-Spectral Matrix (C) defined as

$$C = [\{p(f)p'(f)\}]' \quad (1)$$

where p represents a vector of complex pressures for each microphone, f represents the beamforming frequency and the apostrophe represents the complex conjugate.

A beamforming output is computed over a planar area of space at a known distance from the array (referred to as z -distance). This area is generally centred in line with the centre of the microphone array. The area is evenly discretised into a grid of $NX \times NX$ data points, where NX represents the number of grid lines in the x and y directions. Steering vectors (\hat{v}) are used to scan this area of space under investigation

for noise sources. The steering vectors contain the unique distances of each grid point in the area of investigation to each microphone, m . It is assumed that the wave is emitted from the acoustic source in a spherical distribution. The steering vectors are defined as

$$v(m) = a(m) \frac{r_m(m)}{r_c(m)} \exp \left[\frac{-j2\pi f r_m(m)}{c} \right] \quad (2)$$

$$\hat{v} = [v(1) v(2) \dots v(M)] \quad (3)$$

where a represents a shear layer refraction correction term (Brooks and Humphreys, 2006a), r_m is the distance of the coordinate of the area of investigation grid point to the microphone location, r_c is the distance of the grid point of the area of investigation to the array centre coordinate and c is the speed of sound. The variable m ranges from 1 to M , where M is the total number of microphones in the array. The Delay and Sum beamforming output (Y) is computed using

$$Y(\hat{v}) = \frac{(\hat{v}')^T \{ \text{diag}_1(w) [C] \text{diag}_1(w)^T \} (\hat{v}')}{(\sum_{m=1}^M w(m))^2 - \sum_{m=1}^M w(m)} \quad (4)$$

where w represents a microphone shading vector and the superscript T denotes a matrix transpose. Microphone shading allows each microphone pressure magnitude to be manually adjusted during calibration. Zero values of w can be used to eliminate microphones completely, saving computational time and in some circumstances, data acquisition. The ‘diag₁’ function is the creation of a diagonal matrix, where the diagonal elements are the elements of the row vector to which the function is applied.

The Cross-Spectral algorithm is primarily the same as the Delay and Sum algorithm, except the Cross-Spectral matrix diagonal terms are removed as shown in Equation 5. This eliminates microphone self-noise, which is auto-correlated noise between each microphone. Only the cross-correlated noise is required in beamforming, since the acoustic pressure and phase of the acoustic source arriving at each microphone should have a negligible correlation. The Cross-Spectral beamforming output (Y) is computed using

$$Y(\hat{v}) = \frac{(\hat{v}')^T \{ \text{diag}_1(w) [C - \text{diag}_2(C)] \text{diag}_1(w)^T \} (\hat{v}')}{(\sum_{m=1}^M w(m))^2 - \sum_{m=1}^M w(m)} \quad (5)$$

where the ‘diag₂’ function sets the matrix elements to zero, except along the diagonal.

Brooks and Humphreys (2006a) derived a deconvolution algorithm which further refines the noise source distribution output. DAMAS helps remove the uncertainty of locating and quantifying noise sources by significantly removing sidelobe distributions and refining the source location area. The DAMAS solution scheme is derived by solving the following matrix equation

$$AX = Y \quad (6)$$

where Y is the Delay and Sum or Cross-Spectral output, and X is the DAMAS solution to be solved. The matrix X contains only the true noise sources responsible for the values of Y (Brooks and Humphreys, 2006a). Both matrices X and Y are square and have dimension $NX \times NX$. The matrix A is defined as

$$A_{n,ns} = \frac{\hat{v}_n' \{ \text{diag}_1(w) [G_{ns} - \text{diag}_2(G_{ns})] \text{diag}_1(w)^T \} \hat{v}_n}{(\sum_{m=1}^M w(m))^2 - \sum_{m=1}^M w(m)} \quad (7)$$

where n and ns are independent variables which range from 1 to N , where N is the total number of grid points in the area of investigation (equivalent to $(NX + 1)^2$). The G matrix is defined as a Steering Vector Matrix Array

$$G_n = \begin{bmatrix} (v(1)^{-1})v(1)^{-1} & \dots & (v(1)^{-1})v(M)^{-1} \\ \vdots & \ddots & \vdots \\ (v(M)^{-1})v(1)^{-1} & \dots & (v(M)^{-1})v(M)^{-1} \end{bmatrix}_n \quad (8)$$

Due to its low rank, the A matrix is generally unable to be inverted. Brooks and Humphreys (2006a) derived a tailored iteration scheme to invert the A matrix and thus determine the DAMAS noise source pressures. Equations 9 through 11 detail this inversion procedure. Note that the superscript i denotes the iteration number of the solution scheme.

$$A_{n,1}X_1 + A_{n,2}X_2 + \dots + A_{n,N}X_N = Y \quad (9)$$

$$X_n = Y_n - \left[\sum_{ns=1}^{n-1} A_{n,ns}X_{ns} + \sum_{ns=n+1}^N A_{n,ns}X_{ns} \right] \quad (10)$$

$$X_n^{(i)} = Y_n - \left[\sum_{ns=1}^{n-1} A_{n,ns}X_{ns}^{(i)} + \sum_{ns=n+1}^N A_{n,ns}X_{ns}^{(i-1)} \right] \quad (11)$$

While the output of DAMAS is preferred over the Cross-Spectral results, the DAMAS solution scheme is computationally expensive, sometimes taking several hours to compute for even small array sizes (such as a 16 microphone array). This technique requires many matrix inversion iterations (up to 5000), where the A matrix dimensions can be as high as 2601×2601 (Brooks and Humphreys, 2006a).

Brooks and Humphreys (2006b) furthered DAMAS to DAMAS-C, which shows superior source identification and sidelobe level minimisation to DAMAS. However, it has not been considered for the current work as it is even more computationally expensive than DAMAS. Other beamforming algorithms exist, such as DAMAS-2 and DAMAS-3 (Dougherty, 2005) which are exceptionally fast for the quality of resolution. However, these mathematical algorithms are not publicly available.

It was therefore decided to only perform DAMAS simulations to beamforming cases where the Cross-Spectral technique did not display sufficient source identification. In the case of single monopole source simulation testing, the Cross-Spectral technique is sufficiently accurate to compare the resolution and overall ability of one array design to the other.

BEAMFORMER DESIGN AND OPTIMISATION

The optimal array design for an aeroacoustic testing facility is dependent upon various parameters, including:

- Noise frequencies of investigation
- Size of area of investigation
- Allowable dimensions of the array
- Distance of the array to the noise sources
- Distance between noise sources under investigation
- Maximum allowable sidelobe levels

Many of these parameters are driven by spatial and budget constraints: An optimal array cannot be selected prior to investigation of the items listed above (Underbrink, 2002).

Array Design

Various logarithmic spiral arrays incorporating 63 microphones were investigated using simulations of a monopole noise source located 600mm from the array centre (this cor-

responds to the distance of the airfoil trailing edge to the array in the AWT). Most of the array designs presented adequate resolution of the noise source, displaying a defined main lobe with little sidelobe interference. However, many of these arrays were larger than a square metre in size. In some cases, the theoretical microphone locations were too close to each other, preventing any real installation of microphones without physical interference.

To achieve improved sidelobe distributions and similar beamforming output characteristics using the Cross-Spectral technique, a modification to the spiral was performed to ensure that 63 microphones could be placed in a 700mm \times 700mm square area. This was done by ‘‘squashing’’ the spiral pattern in the direction of the furthest microphone from the array centre. The parametric equations for the coordinates (x and y) of a logarithmic spiral are

$$x(m) = a \cos(\theta(m)) \exp(b\theta(m)) \quad (12)$$

$$y(m) = a \sin(\theta(m)) \exp(b\theta(m)) \quad (13)$$

where a and b are coefficients which affect the overall size of the spiral and how rapidly the arms of the spiral expand from the centre respectively. The angle $\theta(m)$ is defined as

$$\theta(m) = \left(\frac{(m-1)\varphi n}{M} \right) \quad (14)$$

where φ is the spiral sweep angle (i.e. $\varphi = 2\pi$ represents one spiral revolution) and n is the number of sweeps of φ .

Arcondoulis Spiral

The Arcondoulis Spiral coordinates (x' and y') are created by including scaling factors which are a function of m . This is done by including an additional multiplicative to Equations 12 and 13 such that

$$x'(m) = \left[\frac{(m + \epsilon_x M)}{M} \right] a \cos(\theta(m)) \exp(b\theta(m)) \quad (15)$$

$$y'(m) = \left[\frac{(m + \epsilon_y M)}{M} \right] a \sin(\theta(m)) \exp(b\theta(m)) \quad (16)$$

where ϵ_x and ϵ_y are coefficients which determine the ‘‘squashing’’ of the spiral in the x and y directions respectively. In this case, m ranges from 2 to M and $x(1) = y(1) = 0$, to ensure that a microphone is located at the origin. Effectively, the spiral size coefficient is no longer constant and now a function of the number of microphones. In the case of the Arcondoulis array presented in this paper, the parameters were

$$a = 0.03, b = 0.06, n = 6, \varphi = 2\pi, M = 63, \epsilon_x = \epsilon_y = 0.9.$$

The Arcondoulis spiral allows a greater distribution of microphones near the array centre for a given spiral area. However, four microphones located closest to the array centre (excluding the microphone located at the centre of the array) do not fit Equations 15 and 16. This is due to the nature of both the Arcondoulis and the logarithmic spiral, which do not have an element at or near the origin. To ensure that a smooth continuous pattern of microphones was generated, these microphones were manually shifted toward the array centre. This also helped achieve sufficient clearance between each microphone location. The final array design is shown in Figure 3, including the default logarithmic spiral pattern spanning the same area for comparison.

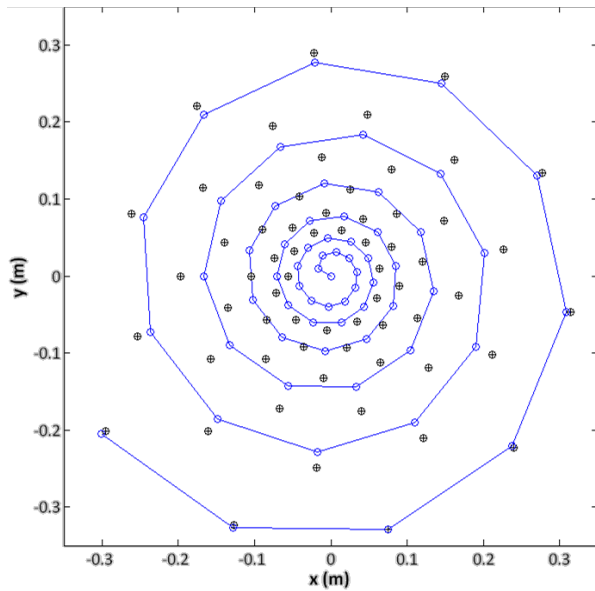


Figure 3: Default Logarithmic Spiral (filled circles) and the Arcondoulis Spiral Microphone Array Design (empty circles, joined by a line). This array pattern is fitted to a plate of size $700\text{mm} \times 700\text{mm}$. The circles identify microphone positions.

Note the differences in the spirals in Figure 3. The Arcondoulis spiral contains a much denser population of microphones near the centre. It also expands more rapidly than the original logarithmic spiral after the spiral arm has made three turns about the centre. This ensures that the same spiral area is covered, also with a greater percentage of microphones near the centre of the array.

Simulation Method

This section details the beamforming simulations used to compare microphone arrays, employing a specialised user-written MATLAB code. A monopole source was simulated as a spherical wave which propagated toward the microphone array, such that each microphone location detected a unique pressure magnitude and phase, which were then input into Equation 1. Equations 2 to 11 were then computed.

Many noise sources of varying frequency and planar location were used to compare array designs using various spiral types. One comparison shown here is for a 3000Hz monopole source, located 600mm from the array centre.

Simulated Array Performance

Figure 4 and Figure 5 show the Cross-Spectral beamforming result of the default logarithmic spiral and the Arcondoulis spiral respectively (as shown in Figure 3). An important array performance parameter in the investigation of airfoil trailing edge noise is the sidelobe distribution. Figure 4 displays several sidelobes which mirror the array pattern (located approximately 0.2m radially from the main lobe centre). The Arcondoulis spiral displays an improved sidelobe distribution away from the main lobe. The sidelobe levels of the Arcondoulis spiral compared to the default spiral are reduced by levels of up to 10dB (for a 3000Hz monopole source).

The investigation of trailing edge noise is highly dependent on the level of sidelobe noise, especially if uncertainty exists surrounding the location of noise sources near or on the trailing edge. In certain aeroacoustic testing regimes, where airfoil leading edge noise is comparable to the trailing edge noise, sidelobe images from both noise sources may constructively interfere. This can lead to confusion in identifying true and false noise sources, especially if a leading edge noise

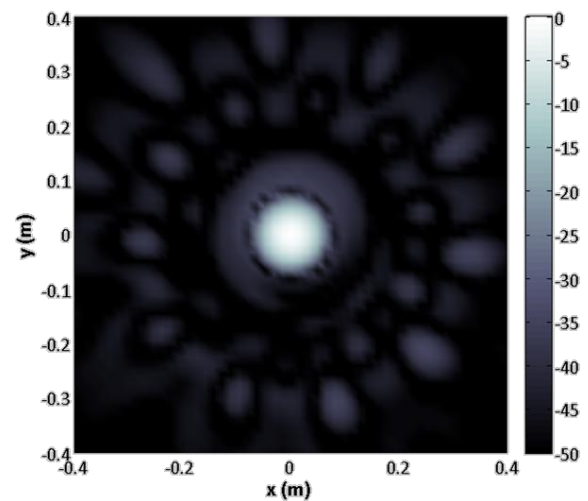


Figure 4: Logarithmic Spiral Cross-Spectral result (normalised dB), for a 3000Hz monopole source located 600mm from the array centre.

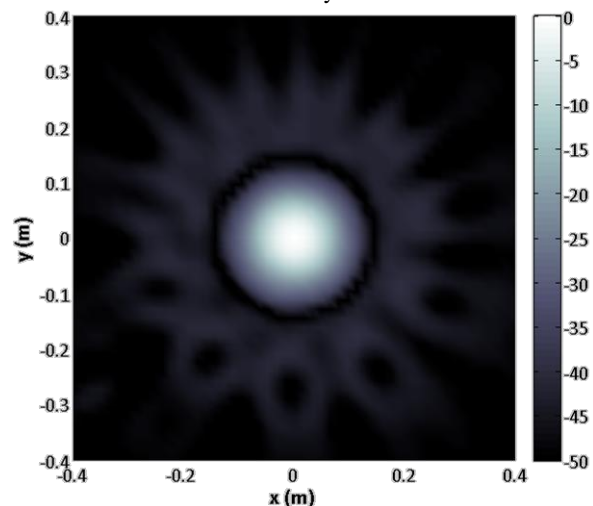


Figure 5: Arcondoulis Spiral Cross-Spectral result (normalised dB), for a 3000Hz monopole source located 600mm from the array centre.

sidelobe is located near or on the trailing edge noise source in a Cross-Spectral image. The superposition of this sidelobe with a trailing edge noise main lobe can be hard to detect and could result in an inaccurate calculation of the trailing edge noise source magnitude using DAMAS.

Another important array performance parameter is the width of the main lobe. While the Arcondoulis spiral shows an improved sidelobe distribution for a 3000Hz monopole source, it also displays a larger main lobe. While this is generally not desirable in beamforming applications which require the identification of a single isolated source, the trailing edge noise will most likely consist of multiple noise sources, corresponding to either several main lobes or a large superimposed main lobe in the Cross-Spectral image. In either case, the trailing edge noise sources can be identified and their total sound pressure level calculated using DAMAS, regardless of the main lobe width.

EXPERIMENTAL PROCEDURE

16 Channel Array

Prior to the manufacture of 63 microphones, it was decided to perform initial tests using a smaller array of 16 microphones. They are located in the microphone provisions of the 63 channel Arcondoulis array, as shown in Figure 6.

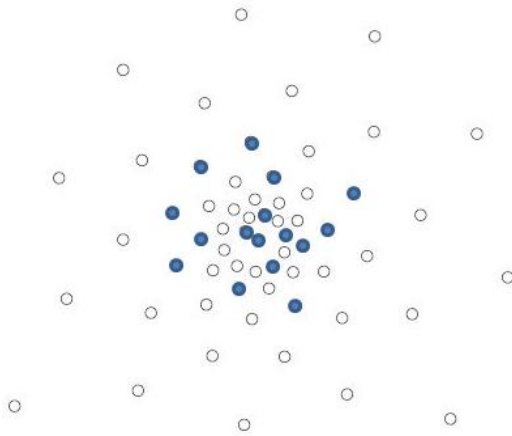


Figure 6: 16 Channel Array microphone locations, depicted by shaded circles. The unshaded circles represent the unused remainder of the array.

Data Acquisition

The data acquisition (DAQ) system used for this study consists of a National Instruments (NI) PXI-1042Q Chassis, with four PXI-4496 DAQ cards. Each card is capable of storing 16 channels of data, thus allowing up to 64 channels of real-time data.

A MATLAB DAQ interface was used to collect this data, which was then run through a Fast Fourier Transform (FFT) to convert the data into the frequency domain. This data is presented in the form of spectral density and also allows the acquisition of the voltage magnitude and phase of each microphone over a frequency range.

The data was acquired at a sampling frequency of 32,768 Hz (2^{15} Hz) for 5 seconds and then band-pass filtered between 50Hz and 10kHz. The noise spectra presented in this paper are taken from the centre microphone of the array, with a frequency resolution of 1Hz and the units are in volts (dB/Hz, relative to 20×10^{-6} volts).

Noise Sources

Various noise sources were used to test the ability of the beamformer to detect noise of varying frequencies and magnitude, both tonal and broadband. For the tonal noise experiments, a frequency of approximately 5000Hz was chosen to test the performance of the array, as this value represents the likely tonal noise frequency of an airfoil in the AWT under near maximum flow conditions (Arcondoulis et al., 2009). This value was determined by the use of the airfoil tonal noise ladder structure equation (Paterson et al., 1973) and verified experimentally. This flow condition and airfoil chord will be the likely experimental conditions for the future work of the aeroacoustic beamformer (see Figure 1) and thus a similar frequency was chosen for preliminary beamforming testing.

Tonal noise sources were synthetically created using computer music production software, called FLStudio 9 (Image-Line Software). The use of synthesisers allowed the generation of sinusoidal, sawtooth and square wave noises, with dominant tones at a frequency of 5275Hz. The noise of each synthesiser was individually exported as audio (.wav) files, which were then uploaded onto an audio playing device (iPod). This audio was then fed directly into externally powered Logitech speakers. While the software spectrum analyser showed a distinct tone at 5275Hz for each noise source, this was checked using a user-written MATLAB spectra code (noise spectra displayed in Figure 8) which acquired the

noise from the speakers. This verified the tonal noise at this frequency.

A small household fan of 160mm diameter was simply chosen as an aeroacoustic broadband noise source. The final beamforming facility set-up is shown in Figure 7, showing the speaker set-up configuration in the Anechoic Chamber, The University of Adelaide. The fan replaced the speakers at that location when it was being tested.

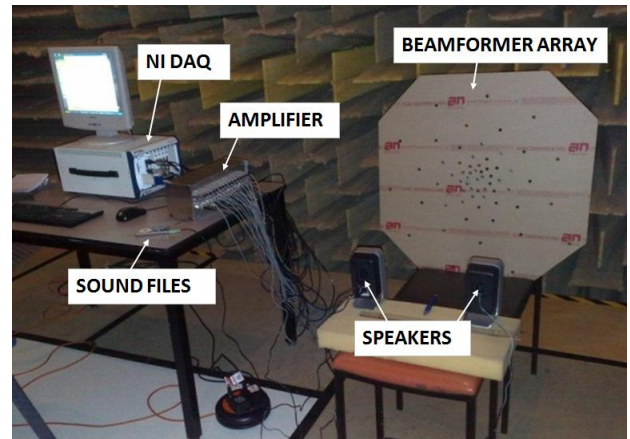


Figure 7: Array testing and calibration set-up.

RESULTS AND DISCUSSION

The following is a summary of some of the beamforming test cases. While the results do not detail a calibration of individual microphones and a sound pressure level evaluation, a simple noise source was used to compare the experimental noise source distributions to those of theoretical monopole sources. This was deemed an adequate first stage of the calibration process.

Sine Wave Source

Using sine waves allowed a direct comparison with simulated results. A 5275Hz sine wave noise was emitted through two speakers, separated by 300mm (x-direction). The line of the speakers was 600mm from the array (z-direction) and the vertical offset of the speaker centres was 100mm (negative y-direction). The spectrum resulting from this noise is shown in Figure 8 and the Cross-Spectral beamforming result is shown in Figure 9.

Figure 8 shows a flat noise spectrum, with the distinct exception of the tone at 5275Hz. Note that at frequencies less than approximately 1000Hz, there is some broadband noise. This is due to the computer cooling fans in the DAQ computer. Figure 9 clearly shows the two separate source regions representing the speakers as noise sources. This beamforming result was compared against the simulated result of a 16 channel array, with identical source locations relative to the array. The simulated result is shown in Figure 10.

In general, there is a good agreement between the measurements and theory. The primary difference between Figure 9 and Figure 10 is the clearer separation of the two noise source regions. At $x = 0$ and $y = -0.1$ in Figure 10, there exist no potential noise sources within 15dB of the noise source strength at the speaker centre, showing greater noise source resolution. In addition, there is a small sidelobe (12dB below the maximum source strength) located at $x = -0.3$, $y = 0.4$ in Figure 9.

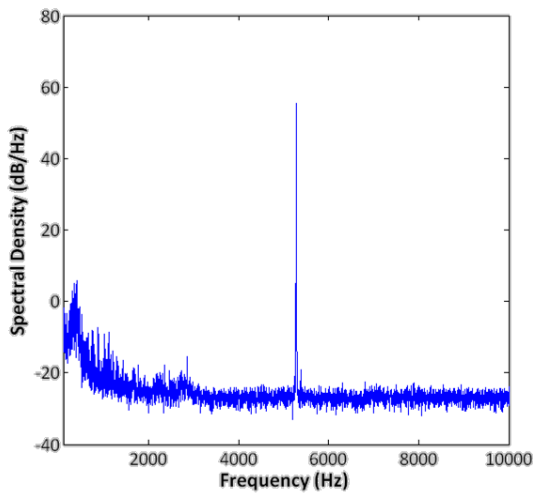


Figure 8: Noise spectra recorded from a 5275Hz tone.

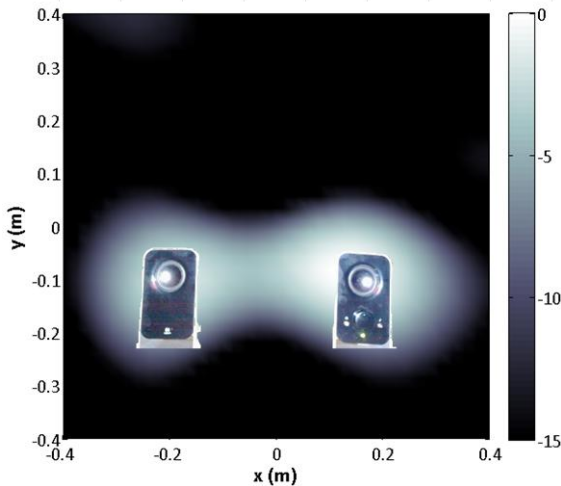


Figure 9: Cross-Spectral beamforming result (voltage dB, normalised to the maximum Cross-Spectral voltage) of two equal strength 5275Hz sine wave sources. An image of the speakers has been superimposed to help show the true source locations.

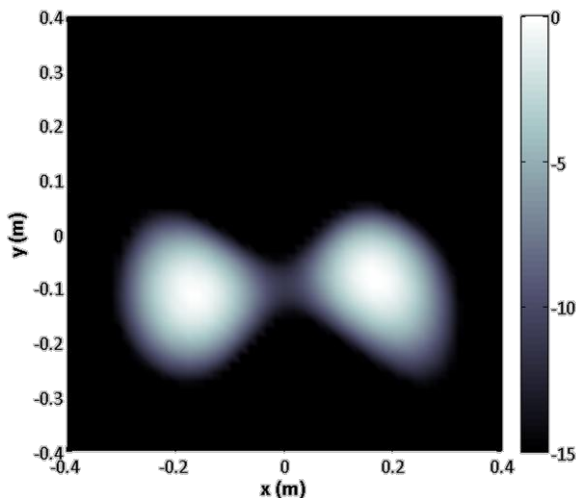


Figure 10: Simulated Cross-Spectral beamforming result for the 16 channel array shown in Figure 6 (in dB, normalised to the maximum Cross-Spectral pressure) of two equal strength 5275Hz sine wave sources.

While the simulated values should match the experimental values, some discrepancy exists. The x , y , and z distances of the speakers to the array were measured by hand, which may lead to some difference in the simulated noise source locations and the true locations. Even a small error in measure-

ment (1mm) can adversely affect the quality of the beamforming result for a 5000Hz noise source (Underbrink, 2002). The speakers are not ideal monopole sources either and may be directional. This would also significantly affect the quality of the beamforming output. These errors will be further investigated during the calibration of the 63 channel array.

Figure 11 shows a beamformer output using the same theoretical simulation conditions as Figure 10, but using the 63 channel array. The noise sources are clearly separated and identifiable, showing the expected improved result to be obtained with a full 63 channel array.

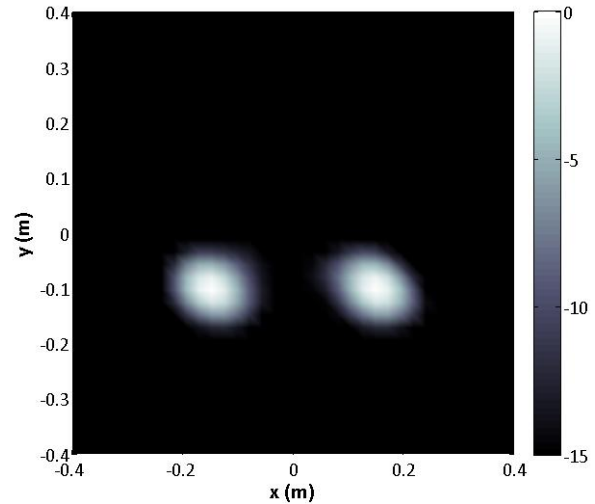


Figure 11: Simulated Cross-Spectral beamforming result for the 63 channel Arcondoulis spiral array shown in Figure 3 (in dB, normalised to the maximum Cross-Spectral pressure) of two equal strength 5275Hz sine wave sources.

Small Fan Noise

A small fan was placed 800mm from the array (z -direction) with its base located 100mm below the y -axis. The fan was run at full speed to create significant aeroacoustic noise. The fan rotated clockwise, so that the top blade of the fan moved towards the beamforming array.

The aerodynamic noise is generated at the trailing edge of the fan, towards the tip where the velocity of the blade is greatest. When turbulent flow on the surface of the fan blade passes the trailing edge, the efficiency of the turbulent acoustic sources close to the edge is increased (Ffowcs Williams and Hall, 1970). To an observer in the acoustic far-field, this creates an effective noise source located at the fan trailing edge with a cardioid-like directivity pattern, as depicted in Figure 12.

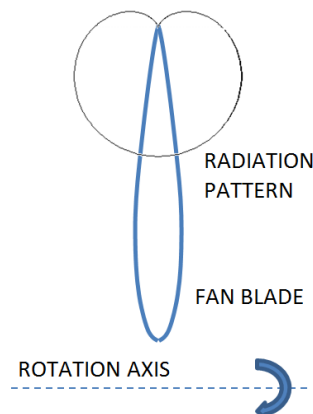


Figure 12: Fan blade noise radiation pattern.

Figure 13 shows the noise spectra of the fan, from 100Hz to 2500Hz, detected at the centre microphone. For frequencies greater than 2500Hz, there was a significant decrease in measured noise. Looking at the frequencies between 1700Hz and 2200Hz, there exists some tonal noise. It was decided to investigate one of these tones to determine the noise source structure at this frequency. Figure 14 shows the selected tone for investigation, being 2050Hz. The frequency of 2050Hz was then beamformed and the Cross-Spectral analysis result is presented in Figure 15.

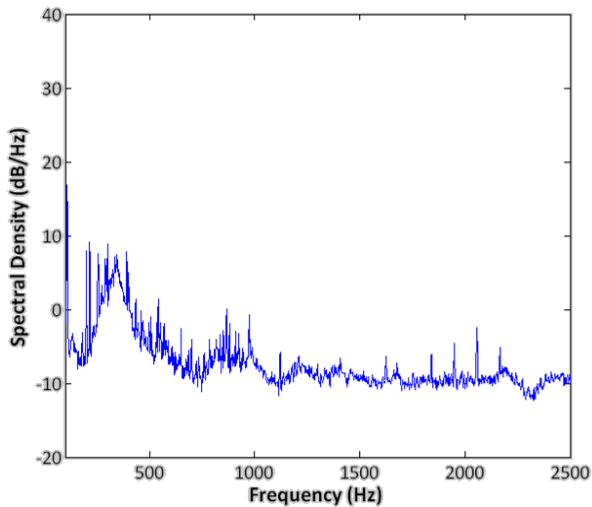


Figure 13: Small fan noise spectra, from 100Hz to 2500Hz.

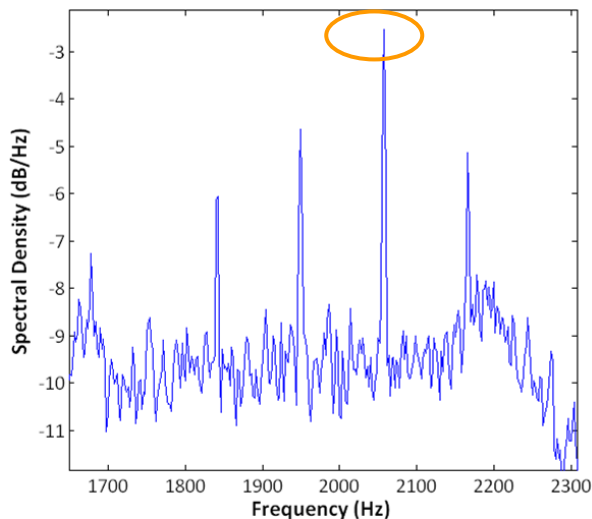


Figure 14: Magnified version of Figure 12, showing peaks in the spectra and ideal tonal frequencies for beamforming investigation. The circled peak is at 2050Hz.

Figure 15 shows an expected noise source distribution. While the exact noise location in this plot is uncertain, the distribution of noise is centred on the upper edge of the fan diameter. The Cross-Spectral solution shown in Figure 15 was created using $N = 1296$ (31×31) grid points in the square area of investigation. This was sufficiently accurate to capture the noise distribution. For lower frequencies, less refined grids can be used to save computational time as the noise source distribution is quite broad. It is unlikely that any of the noise sources will look significantly different in a Cross-Spectral plot if the grid in the area of investigation is refined.

The Cross-Spectral result shown in Figure 15 was then used to create a DAMAS solution, which is displayed in Figure 16. This shows an isolated fan noise source location. The noise source distribution is clear and there is now little uncertainty of the noise source location (as compared to Figure 15, where the noise source location could be within a $\pm 0.1m$ range).

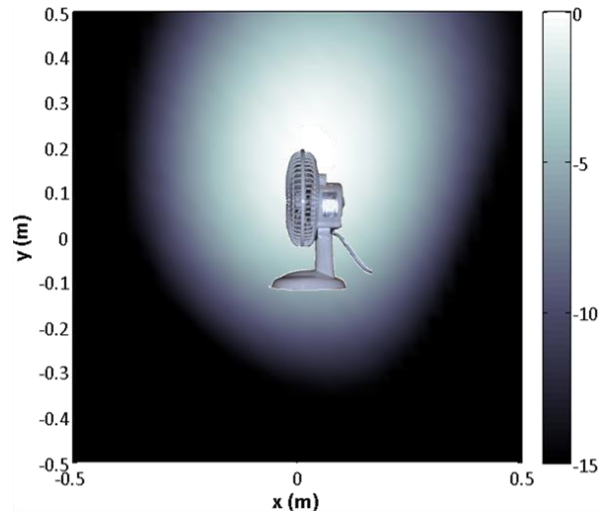


Figure 15: Cross-Spectral beamforming result (voltage dB, normalised to the maximum Cross-Spectral voltage) of a small fan at 2050Hz.

The Cross-Spectral algorithm shows a region of expected noise source, rather than identifying individual sources and does not accurately quantify the sound pressure level at the source locations.

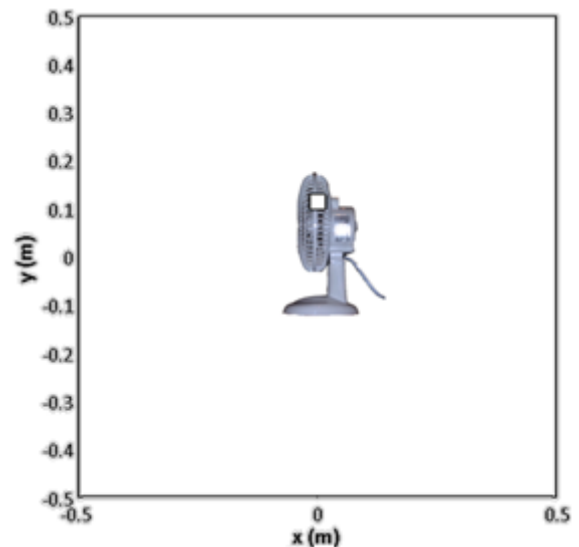


Figure 16: DAMAS beamforming result of a small fan at 2050Hz. All other noise sources are 15dB (voltage dB, normalised to the maximum DAMAS voltage) less than shown.

The solution time for this DAMAS post-processing algorithm was 377s (6mins17s) on a desktop PC. This included a relatively small number of matrix inversion iterations (200). Brooks and Humphreys (2006a) recommend that 5000 iterations may be required for complex noise sources. However, due to the single primary source exhibited in Figure 16, it is expected that the convergence of the solution would be achieved in significantly fewer matrix iterations. The convergence criterion was the norm of the calculated DAMAS pressure value. This value converged within 5×10^{-3} volts.

To test the beamformer at higher frequencies, and also for a non-tonal noise source, a higher arbitrary noise frequency of 3680Hz was chosen for investigation. The noise spectra distribution at this frequency was broadband, with no distinct tones and much lower spectra levels as compared to the 2050Hz case. The Cross-Spectral beamforming result is presented in Figure 17.

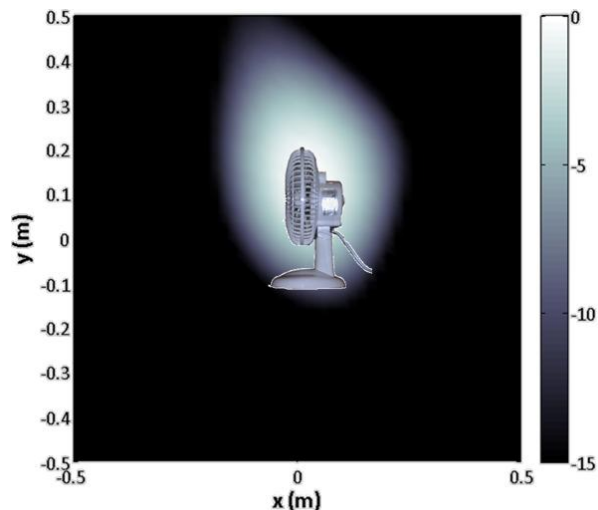


Figure 17: Cross-Spectral beamforming result (voltage dB, normalised to the maximum Cross-Spectral voltage) of a small fan at 3680Hz.

Again, a similar Cross-Spectral noise source distribution is observed. The total area of noise greater than the 15dB threshold is more compact than shown in Figure 15. This is expected as higher noise frequencies display beamforming results with smaller main lobes. In addition, noise sources tend to “beam” at higher frequencies and are much more directional.

A DAMAS solution for this Cross-Spectral result was also performed, using a more refined DAMAS solution scheme. The grid size was more refined $N = 2601$ (51×51) grid points and 5000 matrix inversion iterations were performed, producing a DAMAS norm pressure convergence of 2×10^{-7} volts. The total computation time was large, being 33,245s (9hrs14mins) on a desktop PC. The DAMAS result shown in Figure 18 shows the excellent noise source isolation and accurately locates the fan aeroacoustic noise. Another noise (13dB less than the primary source) was detected near the top of the fan. This may be due to fan motor noise or a reflection of the fan noise from the fan casing.

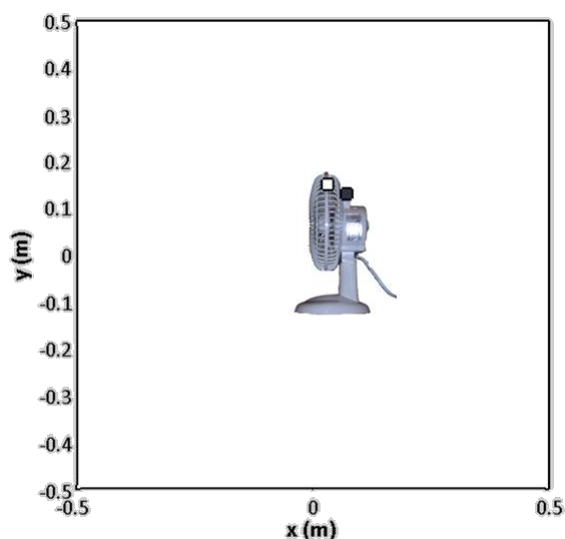


Figure 18: DAMAS beamforming result (voltage dB, normalised to the maximum DAMAS voltage) of a small fan at 3680Hz.

CONCLUSION

The beamforming array design presented shows a subtle alternative to the typical logarithmic spiral used for acoustic

beamforming arrays. The Arcondoulis spiral allows a greater population of microphones near the array centre for a given square area while ensuring a microphone is located in the array centre and covers a defined square area.

The array successfully detected and accurately located both tonal and broadband noise sources. The detection of two coherent monopole sources closely matched theoretical estimates, providing confidence of the ability of the array to locate separate sources. The final calibration of the array is pending the installation of the microphones as well as sound pressure level evaluation of noise sources. This is future work to be performed prior to the installation of the beamformer array in the AWT.

ACKNOWLEDGEMENTS

The authors would like to thank the School of Mechanical Engineering at the University of Adelaide for access and use of the facilities and equipment detailed in this paper.

The authors would also like to extend their sincere gratitude toward Mr. Silvio De Ieso and Mr. Norrio Itsumi for their insight and tireless work in the electronics workshop. Without their efforts, the construction of a 63 channel microphone array would not be possible.

REFERENCES

1. Arcondoulis, E., Doolan, C. and Zander, A., “Airfoil Noise Measurements at Various Angles of Attack and Low Reynolds Number”, Acoustics 2009, 23-25 November 2009, Adelaide, Australia.
2. Brooks, T. and Humphreys, W., “A Deconvolution Approach for the Mapping of Acoustic Sources (DAMAS) determined from Phased Microphone Arrays”, *J. Sound Vib*, **294**, 856-879 (2006a).
3. Brooks, T. and Humphreys, W., “Extension of DAMAS Phased Array Processing for Spatial Coherence Determination (DAMAS-C)”, AIAA 2006-2654, 12th AIAA/CEAS Aeroacoustics Conference, May 8-10, 2006, Cambridge, MA (2006b).
4. Brüel & Kjær, *Technical Review - Beamforming, No. 1 2004*, Brüel & Kjær Sound & Vibration Measurement A/S (2004).
5. Dobrzynski, W., Ewert, R., Pott-Pollenske, M., Herr, M. and Delfs, J., “Research at DLR towards Airframe Noise Prediction and Reduction”, *Aerospace Science and Technology*, **12**, 80 – 90 (2008).
6. Dougherty, R., “Extensions of DAMAS and Benefits and Limitations of Deconvolution in Beamforming”, AIAA 2005-2961, 11th AIAA/CEAS Aeroacoustics Conference (26th AIAA Aeroacoustics Conference), 23 - 25 May 2005, Monterey, California.
7. Ffowes Williams, J.E. and Hall, L.H., “Aerodynamic Sound Generation by Turbulent Flow in the Vicinity of a Scattering Half Plane”, *J. Fluid Mech*, **40**, 657-670 (1970).
8. Oerlemans, S., Fisher, M., Maeder, T. And Kögler, K., “Reduction of Wind Turbine Noise Using Optimized Airfoils and Trailing-Edge Serrations”, *AIAA Journal*, **47**, No. 6 (2009).
9. Paterson, R., Vogt, P., Fink, M. and Munch, C., ‘Vortex Noise of Isolated Airfoils’, *J.Aircraft*, **10**, No. 5 (1973).
10. “Aeroacoustic Phased Array Testing in Low Speed Wind Tunnels” in *Aeroacoustic Measurements* ed. Mueller T.J., (Springer-Verlag Berlin Heidelberg New York, 2002) pp. 98-140.